Geoderma 312 (2018) 74–85

Contents lists available at ScienceDirect

Geoderma

journal homepage: www.elsevier.com/locate/geoderma

Difference between near-surface air, land surface and ground surface temperatures and their influences on the frozen ground on the Qinghai-Tibet Plateau

Dongliang Luo[a,*], Huijun Jin[a,b], Sergey S. Marchenko[a,c], Vladimir E. Romanovsky[c]

[a] State Key Laboratory of Frozen Soil Engineering, Northwest Institute of Eco-Environment and Resources, Chinese Academy of Sciences, Lanzhou 730000, China
[b] School of Civil Engineering, Harbin Institute of Technology, Harbin 150090, China
[c] Permafrost Laboratory, Geophysical Institute, University of Alaska Fairbanks, Fairbanks, Alaska, USA

ARTICLE INFO

Editor: M. Vepraskas

Keywords:
Near-surface air temperature (T_a)
Land surface temperature (*LST*)
Ground surface temperature (*GST*)
Elevational permafrost
Qinghai-Tibet Plateau (QTP)

ABSTRACT

Surface temperature is critical for the simulation of climate change impacts on the ecology, environment, and particularly permafrost in the cryosphere. Virtually, surface temperatures are different in the near-surface air temperature (T_a) measured at a screen-height of 1.5–2 m, the land surface temperature (*LST*) on the top canopy layer, and the ground surface temperature (*GST*) 0–5 cm beneath the surface cover. However, not enough attention has been concentrated on the difference in these surface temperatures. This study aims at quantifying the distinction of surface temperatures by the comparisons and numerical simulations of observational field data collected in a discontinuous permafrost region on the northeastern Qinghai-Tibet Plateau (QTP). We compared the hourly, seasonal and yearly differences between T_a, *LST*, *GST*, and ground temperatures, as well as the freezing and thawing indices, the *N*-factors, and the surface and thermal offsets derived from these temperatures. The results showed that the peak hourly *LST* was reached earliest, closely followed by the hourly T_a. Mean annual *LST* (*MALST*) was moderately comparable to mean annual T_a (*MAAT*), and both were lower than mean annual *GST* (*MAGST*). Surface offsets (*MAGST-MAAT*) were all within 3.5 °C, which are somewhat consistent with other parts of the QTP but smaller than those in the Arctic and Subarctic regions with dense vegetation and thick, long-duration snow cover. Thermal offsets, the mean annual differences between the ground surface and the permafrost surface, were within − 0.3 °C, and one site was even reversed, which may be relevant to equally thawed to frozen thermal conductivities of the soils. Even with identical T_a (comparable to *MAAT* of − 3.27 and − 3.17 °C), the freezing and thawing processes of the active layer were distinctly different, due to the complex influence of surface characteristics and soil textures. Furthermore, we employed the Geophysical Institute Permafrost Lab (GIPL) model to numerically simulate the dynamics of ground temperature driven by T_a, *LST*, and *GST*, respectively. Simulated results demonstrated that *GST* was a reliable driving indicator for the thermal regime of frozen ground, even if no thermal effects of surface characteristics were taken into account. However, great biases of mean annual ground temperatures, being as large as 3 °C, were induced on the basis of simulations with *LST* and T_a when the thermal effect of surface characteristics was neglected. We conclude that quantitative calculation of the thermal effect of surface characteristics on *GST* is indispensable for the permafrost simulations based on the T_a datasets and the *LST* products that derived from thermal infrared remote sensing.

1. Introduction

The research on the permafrost-climate relationship has received extensive and continuous attention since the establishment of geocryology (Yershov, 2004; Zhou et al., 2000). It aims at quantifying the combined interplay of macroscopic factors and the local surface characteristics on the thermal regime of the active layer and permafrost. The macroscopic factors generally consist of climatological and geographical elements, including latitude, elevation, the contrast of ocean-land distribution, general atmospheric circulations, and so forth (Zhang et al., 2008). These factors radically determine the geographical distribution of the magnitude and amount of solar radiation balance on the globe. The local surface characteristics primarily consist of microtopography, surface cover that contains vegetation and snow cover, local hydrology and lithology, and so on (Cheng, 2004). These factors in combination result in a complex energy exchange on the ground

* Corresponding author.
E-mail address: luodongliang@lzb.ac.cn (D. Luo).

http://dx.doi.org/10.1016/j.geoderma.2017.09.037
Received 22 March 2017; Received in revised form 12 September 2017; Accepted 23 September 2017
Available online 18 October 2017

surface, which characterizes the temperature regime and freezing/thawing processes of the ground and the heterogeneity of the occurrence of permafrost.

It is generally believed that permafrost originates and is retained only when the mean annual surface temperature is below 0 °C (Muller et al., 2008), while exactly what threshold is adopted for delineating the continuous, discontinuous, sporadic or isolated permafrost varies globally and regionally (Smith and Riseborough, 2002; Zhou et al., 2000). During the past several decades, especially with the recent prevalence of employing the near-surface air temperature (T_a) datasets from the reanalysis datasets and the land surface temperature (*LST*) products from thermal infrared remote sensing, surface temperatures are increasingly used alone or incorporated together with other factors to correlate or simulate the areal distribution and dynamics of permafrost. However, there is little emphasis among the geocryological communities on the distinction of surface temperatures and the varied simulation results driven by contrasting surface temperatures, which may lead to great bias compared to the reality. Overall, there are three kinds of surface temperatures related to the thermal regime of permafrost: the T_a measured at a screen-height of 1.5–2.0m above the ground surface, the ground surface temperature (*GST*) 0–5 cm beneath the surface cover, and the *LST* at the top of the surface cover. Obviously, these three surface temperatures are very different though connected closely to each other through the complex heat exchange processes at the ground surface.

T_a has a long history of being applied to represent the thermal state of permafrost (Yershov, 2004; Zhou et al., 2000). Different mean annual T_a (*MAAT*) and its vertical lapse rate have been employed to detect the spatial distribution of permafrost and to diagnose the response of permafrost to climate change, either regionally or globally (*e.g.*, Cheng et al., 2012; Førland et al., 2004; Gruber, 2012). The reason why different *MAAT* isotherms are employed to delineate the continuity of permafrost is the thermal effect of surface characteristics and substrates (Cheng, 2004; Smith and Riseborough, 2002). *MAAT* is only one of the important factors influencing the existence and dynamic of permafrost (Muller et al., 2008). The proxy of *MAAT* indicating the occurrence of permafrost should also be taken into full consideration cautiously because of other key factors, such as the snow cover and vegetation at local scales.

GST is measured at the atmosphere-lithosphere interface and is not substantially influenced by wind and shortwave radiation. Due to the thermal effects of all canopy elements, mean annual *GST* (*MAGST*) varies with a wide range within a short distance, even though the *MAAT* is identical (Hasler et al., 2015; Smith, 1975). Thermal influences of these factors on a yearly basis are manifested as the surface offset, the difference between the *MAAT* and the *MAGST* (Smith and Riseborough, 2002). Recently, the field investigation of permafrost assisted by monitoring of *GST* with inexpensive miniature data loggers has been increasing greatly in mountainous areas (*e.g.*, Etzelmüller, 2013; Hasler et al., 2015).

The land surface or skin temperature is assumedly regarded as the temperature coming from the top canopy layer (Bense et al., 2016). *LST* has been successfully retrieved from the satellite-infrared sensors such as the Advanced Very High-resolution Radiometer (AVHRR) and the Moderate Resolution Imaging Spectroradiometer (MODIS) onboard satellites. A methodological approach that fits a sinusoidal model over the daily product is usually adopted to smooth the temporal average of *LST* (Tedesco, 2015). This facilitates the investigation of mountainous permafrost, especially for sparsely and unevenly monitored remote areas (Hachem et al., 2009; Ran et al., 2015). However, in comparison to the difference between *GST* and T_a, the difference between *GST* and *LST* result not only from the influence of the soil/litter layer and surface characteristics but also from the periodicity of shortwave radiation emitted by the sun. Therefore, a significant deviation or bias could be brought when using the *LST* products, due to the insufficient consideration of the buffering effects of vegetation, snow cover, and upper soil layers (Tedesco, 2015).

The ground surface is considered to be a thermal boundary, in addition to a physical boundary of permafrost, on which complex heat and water exchange occurs between the atmosphere and lithosphere (Riseborough et al., 2008; Smith and Riseborough, 2002). The complex interplay between *GST* and T_a is simplified as surface offset and N-factors (Lunardini, 1978; Riseborough et al., 2008). *N*-factors are the ratios between the ground surface freezing index (or thawing index) and air freezing index (or thawing index), which is fundamental to physical or empirical permafrost models (Riseborough et al., 2008). Studies showed that the incorporation of *N*-factors in a standard solution for thaw depth significantly improved the estimation of the active layer thickness (*ALT*) throughout the study areas (Karunaratne and Burn, 2004). However, a number of model practices, especially when applied in vast regions, define the upper boundary conditions with the easily obtained T_a. Moreover, few practices had been conducted to compare the results from different models or simulations based on varied upper boundary conditions. Therefore, there is a pressing need that the surface temperatures undergo an inspection of comparisons before being applied at a finer or local scale.

The Qinghai-Tibet Plateau (QTP) is well known as “the roof of the world” and “the Third Pole”, due to its average altitude exceeding 4000 m above sea level. It is the most vastly distributed elevational permafrost not only at the mid-latitudes but also in the world (Zhou et al., 2000). However, the inhospitable and frigid weather, poor logistical accommodations, and unfavorable transportation conditions confine extensive field investigations of the permafrost. Therefore, the exploration of the quantitative relationship between the surface temperatures and ground temperatures are expected to be employed prior to modeling the spatial distribution and temporal dynamic of permafrost. In this study, we aim at comparing the difference in surface temperatures and providing some implications for simulating ground temperature, further contributing to the quantitatively accurate mapping of permafrost in the rugged topographical environments of the QTP.

2. Materials and methodologies

2.1. Study region

The study region is located in the central part of the source area of the Yellow River (SAYR), northeastern QTP (Fig. 1). The SAYR encompasses a catchment area above Duoshixia (34°34.7′ N, 98°19.5′ E, 41,97 m) along the Yellow River (Jin et al., 2009). As it is located at the fringe of predominantly continuous northeastern QTP and a mosaic transition zone of the discontinuous, sporadic, and isolated permafrost and the seasonally frozen ground, the permafrost in the SAYR is warm and thin. Elevation rapidly increases northwards to 4600 m on the Buqing Mountains and southwards to 5000 m on the Bayan Har Mountains from the central floodplains, where the altitudes are generally within 4350 m. Elevation appears to be the leading factor that controls the spatial differentiation of permafrost. A rapid increase in permafrost temperature was observed with the decrease in elevation on the north slope of the Bayan Har Mountain, until the moderately large area of the seasonally frozen ground with occasionally isolated permafrost in the river valleys and basins. Previous studies showed that permafrost is characterized by the temperature at the depth of zero annual amplitude decreased at a vertical lapse rate of 6 °C/km on the north slope of the Bayan Har Mountains (Luo et al., 2013). In the intermontane depressions and basins at the elevation ranging from 4300 m to 4600 m; however, permafrost temperature varies greatly within a small spatial distance (Li et al., 2016). At a local scale, soil moisture content, surface hydrology, and soil texture together play a decisive role in controlling the thermal regime of permafrost. In this way, the relationship between permafrost and climate is rather complicated.

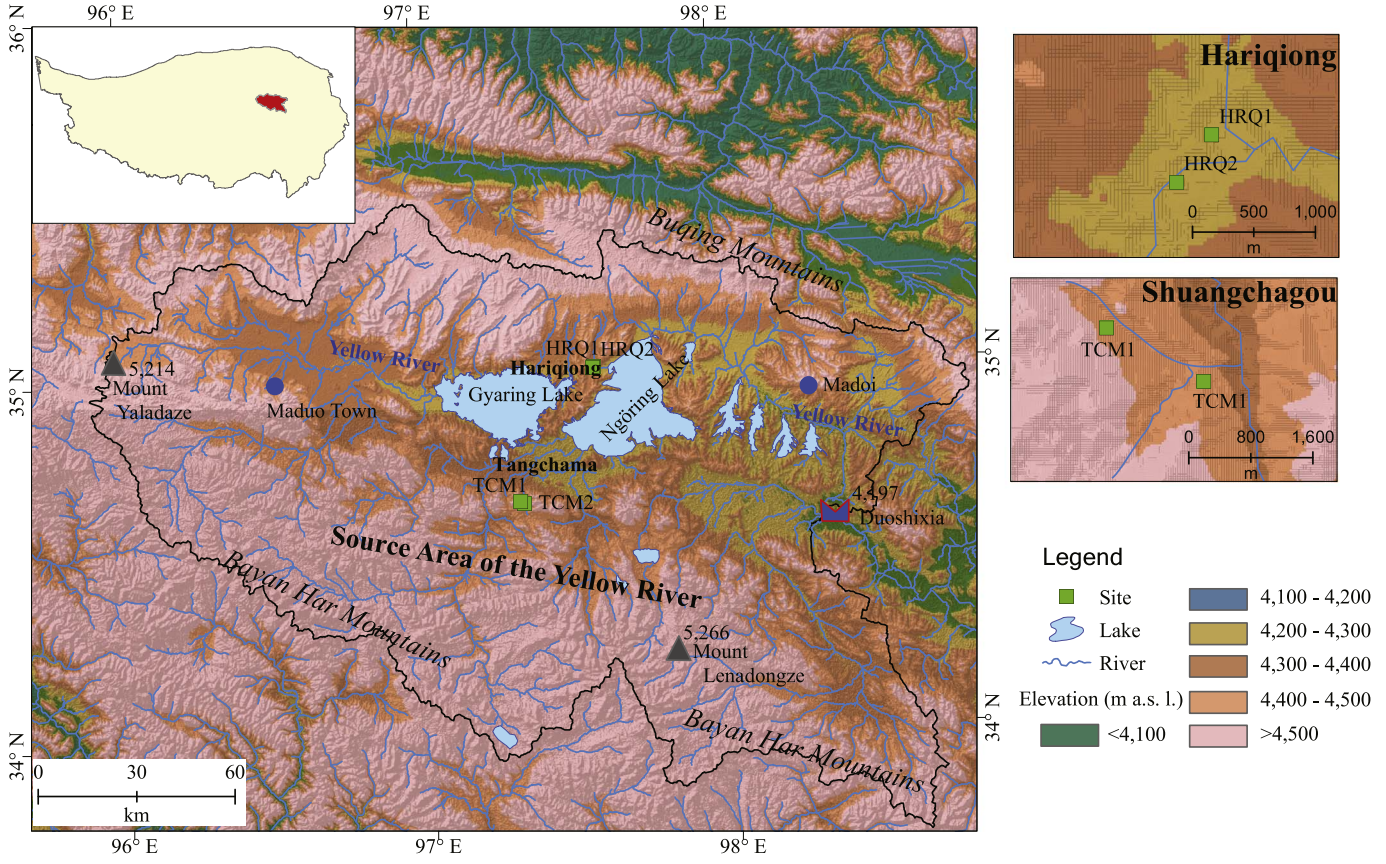

Fig. 1. Study region and the location of study sites in the source area of the Yellow River, Qinghai-Tibet Plateau.

2.2. Site selection and instrumentations

Four *in situ* sites were separately deployed in May 2014 at two geographical units: the HRQ1 (4299 m a. s. l.) and HRQ2 (4301 m a. s. l.) sites at the Hariqiong Basin and the TCM1 (4409 m a. s. l.) and TCM2 (4457 m a. s. l.) sites at the Shuangchagou (2-Forked) Valley (Fig. 1). HRQ1 is rich in saline soil and moderately covered by *Poa annua*. The ground surface at HRQ2 is bare but sparsely dotted by *Polygonum sibiricum* on its periphery, and surrounded by a seasonal pond that freezes in winter and fills with water in summer. TCM1 is densely covered by *Kobresia tibetica*, and TCM2 is also bare on the ground surface. Stratified ground ice with a thickness of 5–10 mm presented at intervals of 1 to 3 mm at depths of 1.3–1.6 m at HRQ2, and a thickness of 3–5 mm presented every 2 to 3 mm at the depths of 1.3–1.5 cm at TCM1. The thermophysical properties of HRQ1, HRQ2, and TCM1 are shown in Table 1, demonstrating the main constituent of fine-grained layers. Thermal properties of the soils were measured by the KD2 Pro thermal properties analyzer (Decagon Scientific Inc.) prior to the installation of sensors and refilling of hand-dug pits of the active layer profile.

The temperature observations were made under the same conditions for all sites. T_a was measured by the Vaisala Temperature/RH probe (HMP155A) installed at a screen-height of 2.0 m above the ground surface. It has an accuracy of ± 0.2 °C. *LST* was measured by the waterproof infrared radiometer sensor (Apogee Instruments Inc., Logan, UT, USA, model SI-111). *LST* was calculated by averaging the temperatures of an oval cast shading over the top canopy layer, *i.e.*, the vegetation surface in summer and the snow surface in winter. The infrared radiometer sensor has a spectral range of 6.5 μm to 14 μm, a 22° half-angle field of view, and a calibration uncertainty of 0.2 °C when the target and detector temperatures are within 20 °C, and 0.5 °C when > 20 °C. The *GST* and ground temperatures within the active layer and permafrost surface were measured by a string of thermistors provided by the State Key Laboratory of Frozen Soil Engineering (SKLFSE), CAS. These thermistors have an accuracy of 0.05 °C. *GST* and ground temperatures were originally collected as the values of electrical resistivity and then transformed into degrees Celsius (°C). All these sensors mentioned above are recorded every 30 min with data loggers (Campbell Scientific, Inc., model CR3000) with electricity supplied by the solar panels. Data from four sites with time series ranging from May 2014 to December 2016 were analyzed in this study.

2.3. Methodologies

We calculated and compared the freezing and thawing indices, surface offset, and thermal offset based on varied surface temperatures. Freezing and thawing indices were calculated as (Lunardini, 1978; Wu et al., 2013):

$$TI = \int_0^{\theta} (T_s - T_f)dt \approx \sum_0^{\theta} \overline{T}\ (T_s > 0^{\circ}\mathrm{C}) \quad (1)$$

$$FI = \int_0^{\theta} (T_s - T_f)dt \approx \sum_0^{\theta} \overline{T}\ (T_s < 0^{\circ}\mathrm{C}) \quad (2)$$

where *TI* and *FI* are thawing and freezing indices, respectively, θ is the length of thawing (freezing) season, T_s and T_f are the surface temperature and the freezing point (0 °C), respectively, and $\overline{T}$ is the daily surface temperature.

Freezing and thawing *N*-factors were calculated on an annual basis for the whole thawing period within a calendar year and the whole freezing period ranging from July to the following June, respectively (Luo et al., 2014; Wu et al., 2013):

$$N_f = \frac{FI_s}{FI_a},\ N_t = \frac{TI_s}{TI_a} \quad (3)$$

Table 1
Thermophysical properties of the soils for selected sites. ρ and θ denote the bulk density and the unfrozen water content, l_t and l_f denote the thawed and the frozen thermal conductivities of the soils, C_t and C_f denote thermal capacities of the soils.

Site	ρ (Mg m^{-3})	θ (%)	l_t	l_f	C_t	C_f	Depth (cm)	Clay (%)	Silt (%)	Sand (%)
			(W m^{-1} K^{-1})		(10^6 J m^{-3} K^{-1})					
HRQ1	1.56	18.1	1.45	1.58	2.07	1.56	0–10	4.1	61.5	34.3
							10–20	7.2	65.1	27.6
							20–30	6.8	69.2	23.9
							30–40	12.8	67.2	19.9
							40–50	7.5	64.2	28.3
HRQ2	1.21	29.7	0.89	1.32	1.89	1.48	0–10	6.0	53.1	40.3
							10–20	7.0	58.1	34.9
							20–30	7.7	51.5	40.8
							30–40	8.7	48.0	43.3
							40–50	6.0	56.3	29.2
TCM2	1.53	26.3	1.72	1.92	2.42	1.87	0–10	4.4	65.9	29.6
							10–20	6.2	70.5	23.3
							20–30	7.8	73.1	19.1
							30–40	10.0	72.9	17.0
							40–50	12.2	72.5	6.7

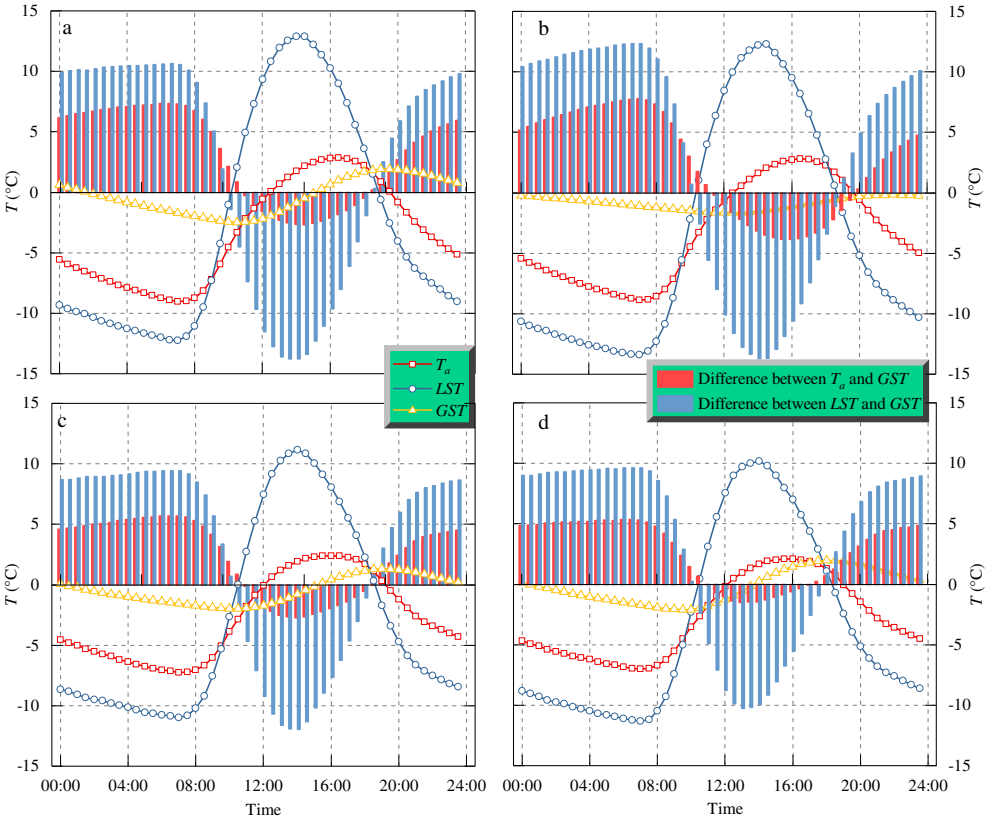

Fig. 2. Half-hourly averaged values of the Ta, the LST and the GST at HRQ1, HRQ2, TCM1 and TCM2 in 2015 and 2016.

where the subscript of *s* represents the ground surface temperature and *a* represents either air temperature or land surface temperature.

The relationships between air, ground surface, and ground temperatures are functionally connected with temperature offsets composed of thermal offset (*TO*) and surface offset (*SO*) (Pan et al., 2016; Smith and Riseborough, 2002; Yin et al., 2017). The surface offset and thermal offset have been utilized as powerful tools for generalizing the permafrost-climate. *SO* and *TO* were calculated with *MAAT*, *MAGST*, and T_{TOP} (mean annual temperature at the bottom of the active layer), which are shown as follows:

$$SO = MAGST - MAAT,\ TO = TTOP - MAGST \quad (4)$$

To compare the influence of T_a, *LST*, and *GST* on the thermal regimes of the ground, we used the Geophysical Institute Permafrost Laboratory (GIPL) model to simulate the ground temperature based on different driving surface temperatures. Thermophysical properties of the soils (soil water content, unfrozen water curve parameters, heat capacity and thermal conductivity, soil layer thickness, *etc.*) were kept the same to consider the sole influence of different surface temperatures. The GIPL model was previously employed at either single points or regions in the Russian and Alaskan Arctic regions (*e.g.*, Jafarov et al., 2013; Marchenko et al., 2008; Nicolsky et al., 2012). It was originally designed to simulate the dynamics of ground temperature under the consideration of the thermal effect of snow cover and the vegetation layer by solving a 1D nonlinear heat equation with phase change numerically (Marchenko et al., 2008). The up-to-date GIPL model employs a finite difference numerical scheme to simulate the dynamics of ground temperature by taking into account the phase change associated

with freezing and thawing processes represented by the unfrozen water curves (Jafarov et al., 2013). In this model, the soil column is divided into several layers with distinct thermophysical properties, and the lower boundary condition of geothermal heat flux was generated using an empirical method (Pollack et al., 1993) for the study site.

To quantify the difference between the simulated and measured ground temperatures, we used the mean absolute error (MAE), the root mean square error (RMSE) and the mean bias error (MBE) to evaluate the model performance and its bias (Willmott and Matsuura, 2005).

$$\mathrm{MAE} = \frac{1}{n}\sum_{k=1}^{n}|e_i|,\ RMSE = \frac{1}{n}\sqrt{\sum_{k=1}^{n} e_i^2},\ \mathrm{MBE} = \frac{1}{n}\sum_{k=1}^{n} e_i \quad (5)$$

The MAE represents a sum of the absolute daily difference between the measured and the simulated ground temperatures over all the days contributing to the average (Jafarov et al., 2013), e_i is a difference between the simulated and measured mean annual ground temperature, and n is the number of observed values.

3. Results

3.1. Difference in surface temperatures

Fig. 2 shows that the differences between the mean half-hourly T_a, *LST*, and *GST* in 2015 and 2016 are evident in the amplitude and the appearance time of peak or valley values. Due to the incapability of shielding from the solar and terrestrial radiation, the oscillation of *LST* was prominently wider than T_a and *GST*. The amplitude of half-hourly *LST* was 20.65, 18.41, 22.73, and 22.75 °C, while the amplitude of half-hourly T_a was 9.20, 8.57, 10.92, and 10.71 °C at TCM1, TCM2, HRQ1, and HRQ2, respectively. Under the influence of the thermal dampening of surface cover and substrates, the amplitude of half-hourly *GST* was only 3.06, 3.94, 3.94, and 1.41 °C at TCM1, TCM2, HRQ1, and HRQ2, respectively.

There is a consistent tendency that the minimum half-hourly *LST* is smaller than that of half-hourly averaged T_a and *GST*, and the maximum half-hourly *LST* is greater than that of half-hourly T_a and *GST* (Fig. 2, Table 2). In general, the *GST* is higher than both the T_a and the *LST* from 0:00 to 10:00 and from 19:00 to 24:00 but is otherwise lower. The differences between the nocturnal *LST* and *GST* were moderately comparable before 8:00 and were approximately 10.3 ± 0.4 °C, 11.6 ± 0.6 °C, 9.1 ± 0.3 °C and 9.3 ± 0.3 °C at HRQ1, HRQ2, TCM1, and TCM2, respectively. In comparison to the differences between T_a and *GST*, the differences between *LST* and *GST* were obviously smaller. The differences between the nocturnal T_a and *GST* before 8:00 were 6.9 ± 0.4 °C, 6.8 ± 0.8 °C, 5.2 ± 0.4 °C, and 5.1 ± 0.2 °C, respectively.

With the complex heat and moisture exchange between the near-surface atmosphere (2 m) and the ground, as well as the increase in longwave radiation that is emitted from the land surface, T_a gradually reached its peak value after *LST*. Peak half-hourly *LST* appears at 14:00 and 14:30, and peak half-hourly T_a appears at 16:00 and 16:30, while that of *GST* appears later than 18:00 (Table 3). The valley value of surface temperature first appeared at approximately 7:00 for half-hourly *LST*, closely followed by the half-hourly T_a at 7:30, and much later for half-hourly *GST*. The underlying surface conditions and the difference in thermophysical properties of the soils dampened the propagation of temperature beneath the ground surface. The time at which the peak value of temperature appeared was influenced by the latent heat exchange between the near-surface atmosphere and the ground surface and the magnitude of reduction of temperature when penetrating into the ground. When temperature was propagated from the land surface into the shallow subsurface ground, the underlying surface cover retarded the increase in temperature, which caused a lag of peak half-hourly *GST*. The first occurrence of the peak value of *LST* is presumably attributed to the direct shortwave solar radiation (Table 3).

Table 2
Maximum (Max), minimum (Min) and annual amplitude (AA) of half-hourly averaged T_a, *LST*, and *GST* in 2015 and 2016.

Site	T_a (°C)			*LST* (°C)			*GST* (°C)		
	Max	Min	AA	Max	Min	AA	Max	Min	AA
TCM1	11.1	− 20.6	31.7	11.1	− 22.1	33.2	8.9	− 11.5	20.5
TCM2	11.4	− 20.0	31.4	14.1	− 25.5	39.5	14.6	− 14.3	28.9
HRQ1	11.4	− 24.2	35.6	14.1	− 28.8	42.9	12.1	− 14.3	26.3
HRQ2	11.4	− 24.0	35.4	13.6	− 28.3	41.9	9.3	− 12.0	21.3

3.2. Difference in surface and thermal offsets

The permafrost-climate relationship is schematically conceptualized in three levels: *MAAT*, *MAGST*, and T_{TOP}. The *MAAT*, *MAGST*, and *MALST* of the four sites are shown in Table 4. *MALST* was moderately comparable to *MAAT* but much lower than *MAGST*. The difference between *MAAT* and *MALST* ranged from − 1.2 °C at TCM2 to 0.9 °C at HRQ1. *MAGST* values were higher than the respective *MALST* at all sites, ranging from 1.8 °C at TCM1 to 3.6 °C at TCM2. This shows a warming effect to T_a by the so-called the buffer layer between the atmosphere and ground surface, which contains the surface vegetation and snow cover and a thin mineral and humus layer (Smith et al., 2005). The differences between *MAAT* and *MAGST* (*i.e.*, the surface offset) for the study sites were all within 3.5 °C, which are comparable to those sites in the interior QTP that lies to the west of the SAYR (Pan et al., 2016), but are lower than those in the Arctic and Subarctic regions, such as Franklin Bluffs and Deadhorse in Alaska that are covered by dense vegetation, particularly closely adhered, thick moss layers (Romanovsky and Osterkamp, 1995). In comparison to the Arctic and Subarctic regions, the thermal effect of surface characteristics, especially the snow cover, on the thermal regime of the ground on the QTP is smaller. Although the snow cover exerts either a warming or cooling effect, and its effect varies daily, monthly and annually, the insulating or warming effect of the snow cover on the ground surface on the QTP is specifically lower than in the Arctic and Subarctic regions, due to less and unstable duration of snow cover by strong solar radiation (Wang and French, 1994).

Thermal offset in the SAYR was small and even vanished, which was 0.12 °C, − 0.22 °C, and − 0.16 °C at TCM1, HRQ1, and HRQ2 (Table 4). This pattern of thermal offset was somewhat consistent with previous reports at the extremely dry sites in other parts of the QTP (Lin et al., 2015; Pan et al., 2016). Relatively lower thermal conductivities in winter due to dry conditions may lead to the lowering of the ratio of frozen to thawed thermal conductivities of the soils (Pan et al., 2016).

The mean annual ground temperature (*MAGT*) becomes progressively colder towards the bottom of the active layer because of the nonlinear effect associated with thawed and frozen thermal conductivities (Goodrich, 1978). However, the lowest *MAGT* may not appear at the bottom of the active layer on the QTP. *ALT* at HRQ1 and HRQ2 were 1.7 m and 1.3 m, respectively, while the lowest *MAGT* appeared at the depth of 0.8 m with a value of − 1.04 °C at HRQ2, and even decreased with the increase of depth in the active layer and permafrost at HRQ1 (Fig. 3). This may also be attributed to the small difference between the thawed and frozen thermal conductivities. For sites in the SAYR, the soil textures are mainly medium sand with a small amount of soil moisture content (Table 1).

3.3. Difference in freezing and thawing indices

The surface roughness and complex surface characteristics may result in a heterogeneity of thawing and freezing indices between different surface temperatures. Generally, the differences between the freezing indices of *LST* and T_a are smaller than that of thawing indices

Table 3
Peak (valley) half-hourly value and appearing time of T_a, *LST*, and *GST* (in 24-h system).

Site	Peak value (hh:mm/°C)						Valley value (hh:mm/°C)					
	T_a		*LST*		*GST*		T_a		*LST*		*GST*	
TCM1	16:00	2.1	14:30	10.1	19:00	0.7	7:30	− 7.1	7:00	− 10.6	10:00	− 2.3
TCM2	16:00	1.6	14:30	7.2	18:00	1.4	7:00	− 7.0	7:00	− 11.2	9:00	− 2.5
HRQ1	16:30	2.5	14:00	11.7	19:00	1.8	7:30	− 8.5	7:00	− 11.1	10:30	− 2.2
HRQ2	16:30	2.4	14:00	10.4	22:00	− 0.07	7:30	− 8.3	6:30	− 12.4	12:00	− 1.5

Table 4
Mean annual surface temperature, surface offset (*SO*) and thermal offset (*TO*).

Site	*MAAT* (°C)	*MALST* (°C)	*MAGST* (°C)	*TTOP* (°C)	*SO* (°C)	*TO* (°C)	*ALT* (m)
TCM1	− 2.88	− 3.09	− 1.25	− 1.13	1.63	0.12	1.2
TCM2	− 3.03	− 4.24	− 0.67	–	2.36	–	–
HRQ1	− 3.27	− 2.36	− 0.23	− 0.45	3.04	0.22	1.7
HRQ2	− 3.17	− 3.67	− 0.74	− 0.90	2.43	0.16	1.3

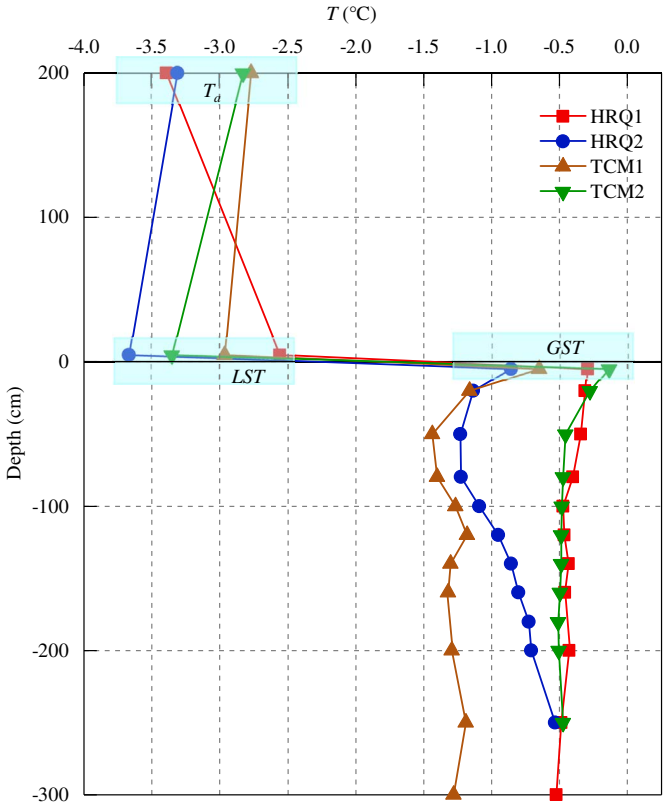

Fig. 3. Profiles of mean annual Ta, GST and ground temperature at TCM2, HRQ1 and HRQ2 in 2015.

Table 5
Annual freezing indices (*FI*) and thawing indices (*TI*).

Site name	Freezing indices (°C d)			Thawing indices (°C d)		
	T_a	*LST*	*GST*	T_a	*LST*	*GST*
TCM-1	1673.2	1881.3	1036.3	682.9	804.0	682.7
TCM-2	1763.5	2370.3	1221.8	654.8	852.4	1059.0
HRQ-1	1928.9	1925.2	1125.8	710.2	1054.0	1033.8
HRQ-2	1920.0	2224.4	1026.0	712.6	888.1	710.9

of *LST* and T_a, while freezing indices of *LST* are larger than T_a, except for HRQ1, which corresponds to the pattern of annual average values (Tables 4 and 5). The annual freezing indices of T_a were comparable to those of *LST* but much higher than those of *GST* among all the sites. This causes different ratios of freezing and thawing indices among *GST*, T_a, and *LST*. The ratio of annual freezing indices among different sites tends to be more analogous than that of annual thawing indices. They were 0.46–0.57 between *GST* and T_a, and 1.03–1.26 between *LST* and T_a. However, the ratio of annual thawing indices of *LST* (T_a) and *GST* was dependent on sites, ranging from 1.00 to 3.24 between *GST* and T_a and from 1.18 to 2.25 between *LST* and T_a in the SAYR.

Surprisingly, freezing indices of T_a and *LST* were equivalent at HRQ1, although the *MALST* was − 1 °C higher than the *MAAT*, which may be attributed to a larger amplitude of *LST* than T_a (Fig. 2). Moreover, T_a was comparable at HRQ1 and HRQ2, which are located in the Hariqiong Basin within a spatial distance of 200 m, while the freezing index of *LST* was 300 °C·d higher at HRQ2 than at HRQ1, and the thawing index of *LST* at HRQ2 was double that of HRQ1. This indicates a larger difference between the surface temperatures in summer than in winter. Therefore, great bias is likely to be brought in when calculating the active layer thickness based on the thawing indices from the *LST* products derived from the thermal infrared remote sensing.

3.4. Difference in within-plot freezing/thawing processes

Regardless of the identical T_a, the freezing and thawing processes of the active layer differed at HRQ1 and HRQ2 (Figs. 4 and 5). At HRQ1, thawing processes started on 17 April 2015, and the thawing front advanced towards the bottom of the active layer (1.5 m) on 10 September 2015. Freezing processes from the bottom of the active layer started on 16 October 2015, and downward freezing from the ground surface commenced five days later. Both freezing fronts joined on 31 October 2015 at the depth of 1.0 m. At HRQ2, thawing processes began on 18 May 2015, which was much later than for HRQ1. The progressive thawing front suspended on 8 October 2015, almost at the same time as for HRQ1. Freezing on the ground surface started on 26 October 2015. Freezing fronts from the bottom and the ground surface of HRQ2 joined on 31 October 2015 at the depth of 0.6 m, which was almost the same time as for HRQ1. Comparatively speaking, the commencement of thawing and freezing of the active layer on the ground surface were distinctively different, but the time of finished thawing of the active layer, and commencement of freezing from the bottom of the active layer were almost the same, which rendered a different thawing duration of 197 and 166 days, respectively.

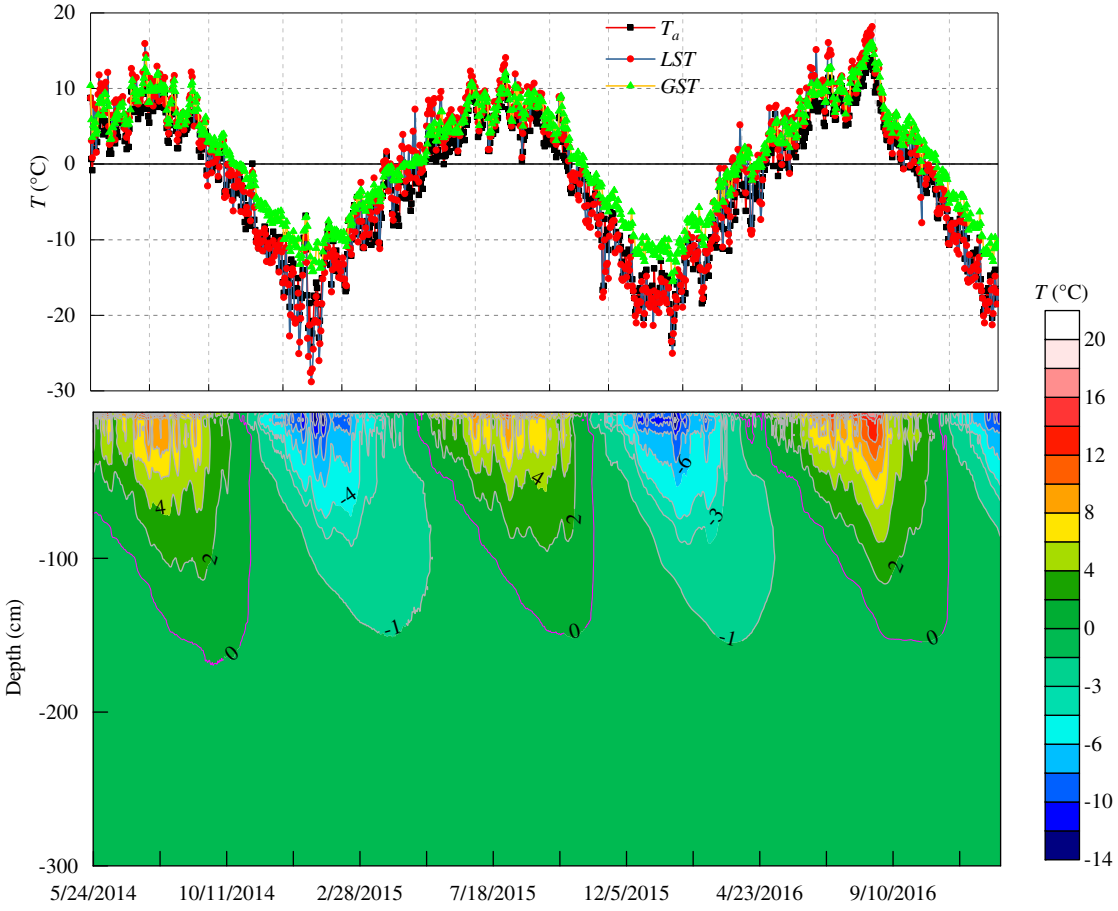

Fig. 4. Variations of T_a, *LST*, *GST*, and freezing and thawing processes at HRQ1 from May 2014 to December 2016.

3.5. Influence on the simulated ground temperatures

We compared the simulated results based on the GIPL model and observed ground temperatures at the depths of 0.2 m, 0.5 m, 0.8 m and 1.2 m at TCM2, HRQ1, and HRQ2 (Figs. 6 through 8). The MAE of simulated ground temperature at TCM2, HRQ1, and HRQ2 is 0.3574, 0.6642, and 0.3436 based upon *GST*, 3.3311, 3.3926, and 3.5306 based on *LST*, and 2.7087, 2.9933, and 2.5828 on the basis of T_a at the depth of 0.2 m. Generally, the MAE of simulated ground temperatures based on *GST* is lower than the simulation based on *LST* and T_a at the depth of 0.5, 0.8, and 1.2 m. This demonstrates that the simulations based upon *GST* were in good agreement with the measured values, while large bias was produced by simulations based upon both T_a and *LST*, especially for shallower depths, at all sites.

The simulations based on *GST* are likely to overestimate the ground temperatures, but they are still reasonable, while the simulations based on *LST* and T_a significantly underestimate the ground temperature, particularly in winter. The simulated *MAGT* based on *GST* was 0.1 to 0.27 °C higher than the measured *MAGT* at TCM2, 0.08 to 0.29 °C higher than the measured ground temperature at HRQ1, and 0.32 to 0.54 °C higher than the measured ground temperature at HRQ2. However, the measured *MAGT* could be at least 1.4 °C higher than the simulated *MAGT* based on *LST*, and at least 2.0 °C higher than the simulated *MAGT* based on T_a. In addition, simulated *MAGT*s based on *GST* correlated well with the measured values, while no clear relationships were found between the measured *MAGT*s and the simulated *MAGT*s based on *LST* and T_a (Fig. 9). This demonstrates that the thermal effect of surface characteristics, *i.e.*, the vegetation and snow cover, and the application of *N*-factors indirectly substituting the T_a, are expected to be prudently adopted before the simulations are implemented. Otherwise, the simulated results based on T_a and *LST* could be much lower than practical observed *MAGT*.

Larger simulated bias in winter than in summer was presented by the simulations based on T_a, *GST*, and *LST* (Figs. 6–8), which indicates that the thermal effect of close-adhered withered vegetation and snow cover is non-negligible for numerical simulations of frozen ground. The difference between the measured and simulated ground temperatures in winter was larger than that in summer. The amplitude of simulated ground temperature was largest based on *LST*, closely followed by that based on T_a. Differences between the highest measured and simulated ground temperatures were all within 4 °C at all depths, while differences between the lowest measured and simulated results based on *GST* were almost the same. However, the difference between the measured value and lowest value of simulated results based on *LST* and T_a could reach as high as 10 °C (Figs. 6 to 8). This demonstrates that the *GST* could be used directly as the input data to simulate the thermal state of permafrost, however, great errors and much thicker *ALT* than in reality could be introduced in the case of simulations directly based on *LST* and T_a.

4. Discussion

4.1. Thermal effect of surface characteristics

The thermal effect of surface characteristics on the ground had been widely documented in Canadian, Alaskan, and Siberian Arctic and Subarctic regions (Fukui et al., 2008; Karunaratne and Burn, 2004; Klene et al., 2013; Romanovsky and Osterkamp, 1995) but relatively seldom reported on the rugged QTP (Pan et al., 2016; Yin et al., 2017), which is the largest area of elevational permafrost in the world. As

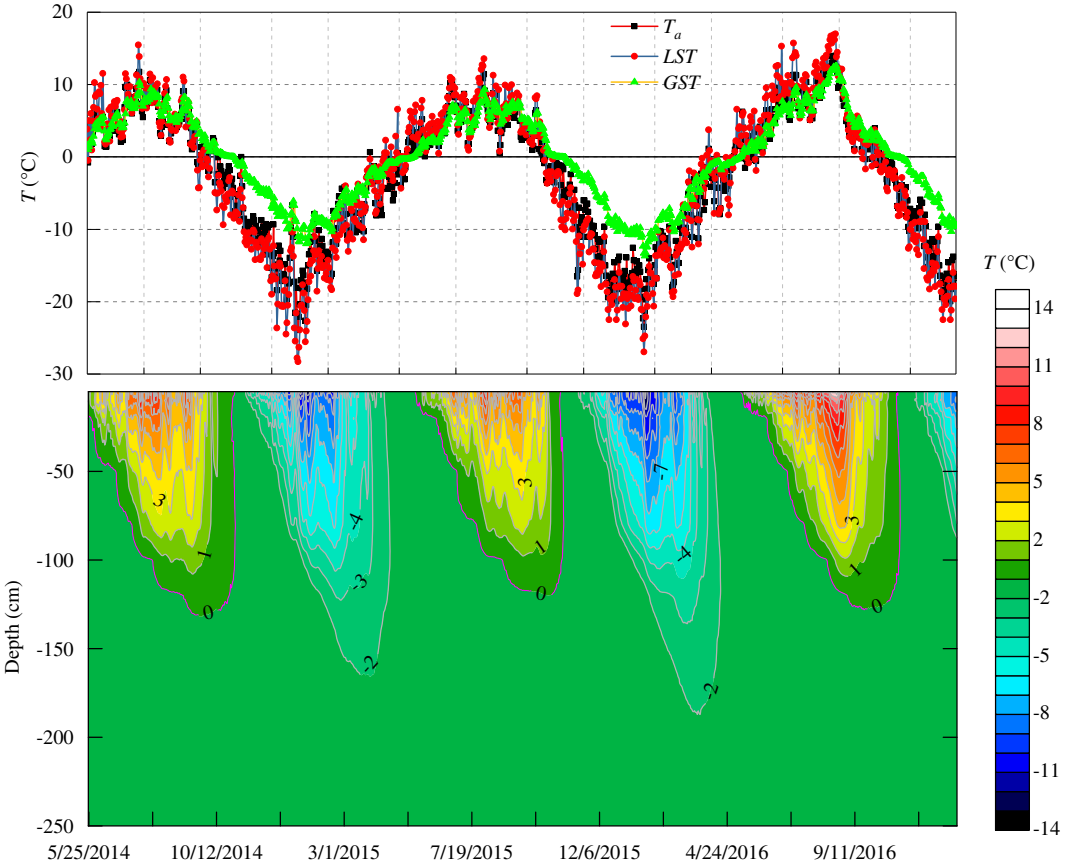

Fig. 5. Variations of T_a, *LST*, *GST*, and freezing and thawing processes at HRQ2 from May 2014 to December 2016.

MAAT is relatively comparable in within-plot (Figs. 4 and 5), the difference in surface offset is generally caused by the spatial differentiation of *MAGST*, due to a strong spatial heterogeneity. The heat-transfer and heat-flow, and phase changes of water on the ground surface and subsurface, and the presence of snow cover in winter all exert great influences on the differentiation of *GST*. Surface offsets could be as large as 6.8 °C at Franklin Bluffs, 6.7 °C at Dead horse, and 3.9 °C at West Dock in the Arctic Alaska (Romanovsky and Osterkamp, 1995). Coincidentally, *MAGST* ranges from 0.8 °C to 4.1 °C at experimental sites of Mayo, Yukon Territory, Canada, while the *MAAT* is comparable (− 2.5 to −2 °C) (Karunaratne and Burn, 2004). In China, the surface offset is smaller in Northeastern China where mainly latitudinal permafrost occurs (Luo et al., 2014). In addition, previous studies in China showed that the surface offsets were 2.0–4.1 °C in the Qinghai Province and 2.0–5.0 °C in the Tibet Autonomous Region, which were higher than those in Northeastern China, including the Heilongjiang Province (0.8–2.8 °C), Liaoning Province (1.0–2.4 °C) and Jilin Province (0.8–2.4 °C) (Xu et al., 2010). However, these climatological values may be quite different from those defined in geocryological studies, due to the measurement of the *GST* on the bare ground surface in summer and the snow surface in winter at Chinese national meteorological stations (Luo et al., 2014). Field observations showed that the surface offsets were relatively consistent on the QTP (Pan et al., 2016; Yin et al., 2017), presumably due to the prevailing bare or relatively sparse vegetation cover and the lack of close-adhered moss layer and thick snow cover.

Essentially, all the three surface temperatures are influenced by the geographical redistribution of the solar radiation emitted by the sun. *GST* is undoubtedly affected by T_a, which is closely related to both macro factors such as latitude, elevation, and land-ocean contrast, and to local factors such as topography, the regime of snow cover, and surface characteristics (Karunaratne and Burn, 2004). Quite a number of studies use the T_a to drive permafrost models under the consideration of the *N*-factors, which were originally developed to summarize the surface energy balance for engineering purposes (Carlson and 223, 1952). The warming or cooling effect provided by the surface characteristics under the reduction of the amplitude of T_a and *LST* to *GST* is likely to be considered with *N*-factors. The annual amplitude of temperature is closely related to the thawing indices, which are the principal parameters for calculating the thawing depth (Riseborough et al., 2008; Romanovsky and Osterkamp, 1995). The neglect of the thermal effect of vegetation layer, snow cover, and moisture on the ground surface temperatures may exaggerate the distribution of permafrost, deepen the active layer thickness, and lower the ground temperatures in comparison to the permafrost in reality. Therefore, building a purposeful monitoring network of *GST* with a cooperative joint scientific team in the rugged QTP is extremely urgent. Related monitoring of T_a and *LST* are also overlooked. As a result, the thermal effect of surface characteristics on the ground temperature is expected to be quantified, and it is hopeful that better results of mapping permafrost are to be achieved.

The role of the snow cover on the QTP plays a subordinative role when compared to that in the Arctic and Subarctic regions. The T_{TOP}, one paramount parameter of the thermal stability of permafrost, was recognized as resulting from the interplay between the surface characteristics, the thermal properties of soils and the T_a (Smith and Riseborough, 2002). The importance of snow cover on the ground in cold Canada even leads to a use of it as a proxy for delineating the continuous and discontinuous permafrost (Smith et al., 2005). On the QTP, snow cover could not be stably formed due to the strong solar radiation, therefore the thermal effect of snow cover is generally neglected for permafrost. However, the extremely frequent solid precipitation (snow or hail), including trace solid precipitation even in summer, may exert significant influence on the thermal regime of the

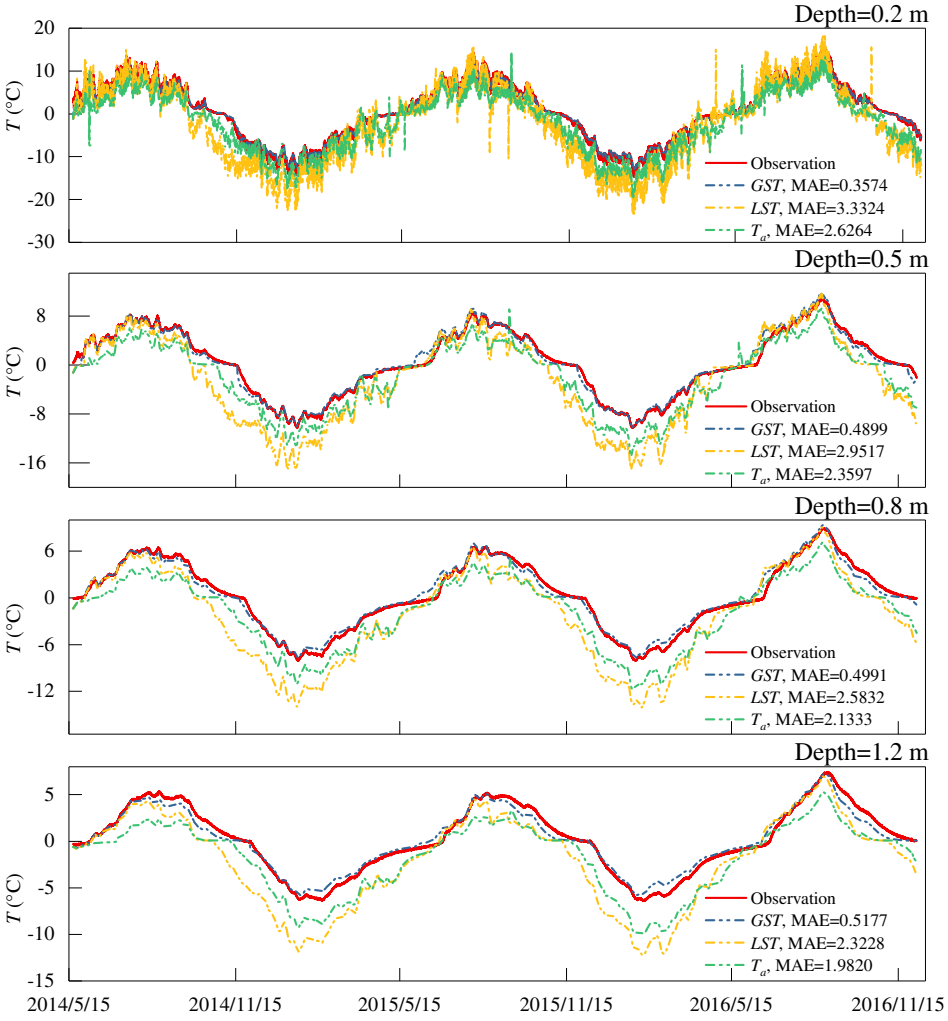

Fig. 6. Measured and simulated results of ground temperature at depths of 0.2, 0.5, 0.8 and 1.0 m at TCM2.

active layer and permafrost through the accumulations of a great amount of snow water equivalent and the exchange of latent heat. Therefore, field experiments of the thermal influence of the regime of the snow cover and its duration on permafrost temperature are expected to be carried out in the future.

Thermal offset mainly results from the difference between the thawed and frozen thermal conductivities, which could be theoretically calculated using a function such as (Romanovsky and Osterkamp, 1995):

$$\frac{N_T{}^* I_T\left(\frac{K_T}{K_F}-1\right)}{P} \tag{6}$$

where N_T is the thawing N-factor, I_T is the thawing index of T_a, and K_T and K_F denote the thawed and frozen thermal conductivities. Numerical simulations by Goodrich (1978) demonstrated that the thermal offset could reach -3 °C when the ratio K_T/K_F is 10. If K_T is slightly smaller than or equal to K_F, the thermal offset will be smaller and the *MAGT* profile would be linear within the active layer (Pan et al., 2016). The soil architectures without or with only thin surface organic horizons on the QTP prominently differ from those in the Arctic and subarctic regions. Factual soil thermo-physical properties demonstrated that the thawed thermal conductivities are comparable to the frozen thermal conductivities (Table 1). The thawed conductivities may be even larger than the frozen thermal conductivities for clayey and gravel loam with a lower content of soil moisture (Xu et al., 2010). Therefore, as for dry clayey and gravel loam on the QTP, the thermal offsets are much smaller or even reversed, and the lowest *MAGT* does not appear at the bottom of the active layer.

4.2. Implications on the thermal regime of frozen ground

The permafrost-climate relationship is composed of T_a, *GST* and the ground temperatures. For *LST*, it is not considered to be a component of the permafrost-climate relationship, although the practices taking *LST* to correlate the occurrence of permafrost increase recently. The thermal effect of vegetation, snow cover, and moisture availability is supposed to be considered prior to permafrost modeling, due to their varied thermal properties on the difference of *GST* and subsurface soil temperatures. Otherwise, the simulated results tend to exaggerate the thermal state of the frozen ground in reality, particularly in winter (Figs. 6 to 8).

We should be aware that the *LST* markedly differs from the *GST* as the crucial influence of surface characteristics. Regardless of the thermal effect of the vegetation layer and snow cover, however, the simulated results based solely on *GST* match highly with the observed ground temperatures. In other words, in the case of taking a single parameter to drive the simulation, *GST* is a much more reliable indicator and the true thermal upper boundary of permafrost models. For T_a and *LST*, great bias may be brought in by the direct use, due to the complex influence of surface characteristics. The thermal effect of surface characteristics is responsible for the significant displacement of *LST* to *GST*, which hampers simply employing *LST* as an effective proxy in a lumped form to delineate the continuity of permafrost.

Differences in surface temperatures remind us to take full accout of

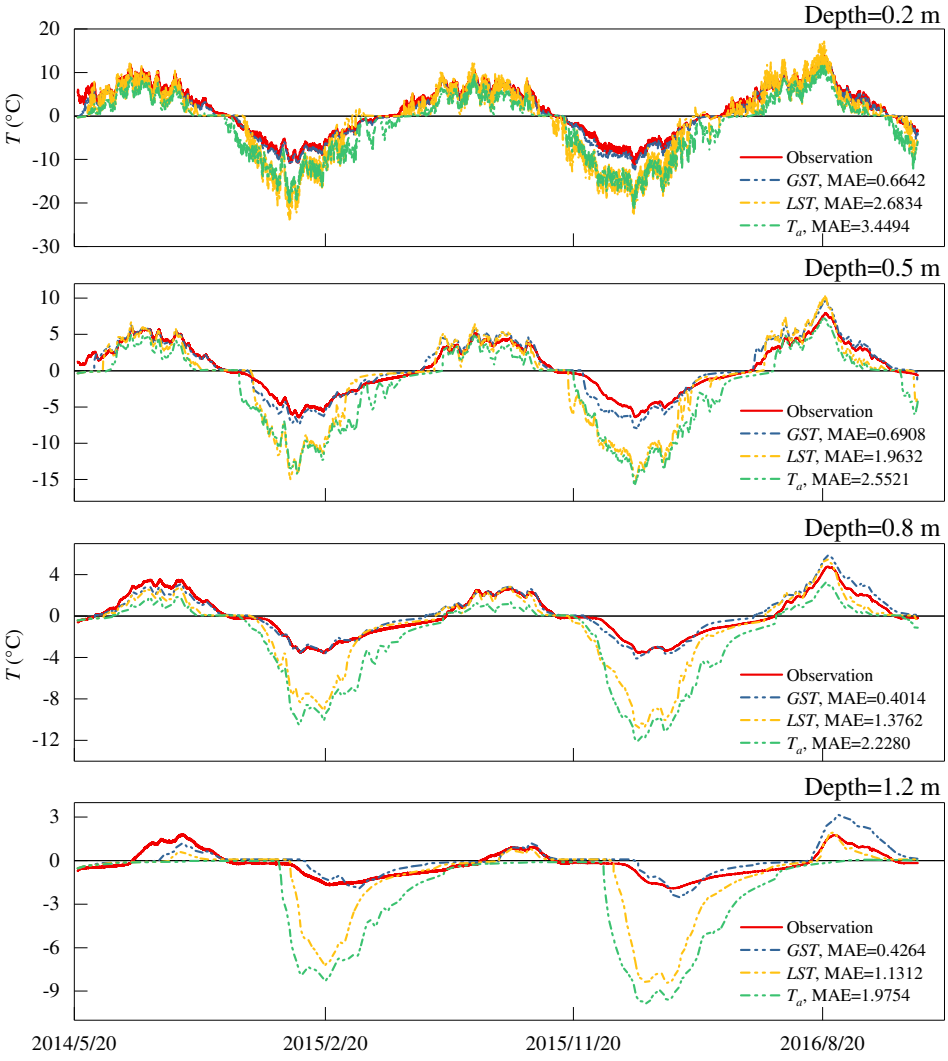

Fig. 7. Measured and simulated results of ground temperature at depths of 0.2, 0.5, 0.8 and 1.0 m at HRQ1.

the thermal effect of surface characteristics upon retrieving the *LST* products and applying them to drive the permafrost models. *LST* even differs prominently from T_a, although the T_a and *LST* are comparable in yearly bases (Fig. 2 and Table 4). On the one hand, the difference between T_a and *LST* is caused by the complex energy exchange in the near-surface boundary layer because of the shortwave radiation and the turbulent exchange. The land surface is first heated by the shortwave radiation emitted from the sun, which causes the *LST* to instantaneously reach the peak value at approximately 2:00 p.m., because the strongest surface radiation occurs two hours after the solar altitude reaches the highest point in the daily rhythms caused by the rotation of the earth. While T_a in the radiation shield does not directly receive the solar radiation from the sun, it is influenced by the longwave radiation undergoing the transmitting, dampening, and reducing of energy emitted from the land surface and the near-surface atmosphere. Based on the thermal radiative transfer theory, the upward longwave radiation emitted by the land surface depends on the *LST*, emissivity and downward longwave radiation (Tedesco, 2015). Therefore, it takes more time for T_a to arrive at the peak value than *LST*. The received amount of energy of emitted longwave radiation usually depends on the content of moisture in the near-surface. Therefore, the amplitude of T_a could be smaller than *LST*, and the time at which the peak and valley values arrive is lagged. On the other hand, vegetation in summer and snow cover in winter on the ground surface present a thermal retarding to *GST* from T_a and *LST*. Therefore, the real upper boundary of the permafrost is the 0–5 cm subsurface beneath the surface covers, rather than the canopy or top layer of vegetation and snow cover.

5. Summary and conclusions

Great differences exist between the air temperature, the land surface temperature, and the ground surface temperature. To compare varied regimes of surface temperatures and their influences on the thermal regime of subsurface frozen ground, we set up four automatic weather stations equipped with sensors for T_a, *LST*, and *GST* in the source area of the Yellow River, northeastern QTP.

As the land surface was first heated by the solar radiation emitted from the sun, the half-hourly surface temperature arrives at the peak value at a time between 14:00 and 15:00 for *LST*, between 16:00 and 17:00 for T_a, and between 18:00 and 22:00 for *GST*. The half-hourly valley value appears almost the same at a time between 6:30 and 7:30 for T_a and *LST* and between 9:00 and 12:00 for *GST*. The annual amplitude is between 33.21 and 42.88 °C for *LST*, between 31.37 and 35.57 °C for T_a, and between 20.47 °C and 28.93 °C for *GST*. The complex energy exchange in the near-surface atmosphere, and the thermal effects of surface characteristics are responsible for the lag of extreme value of *GST*.

The *MALST* is comparable to the *MAAT*; both are much lower than the *MAGST*, which brings in a distinctive difference in surface offset. Surface offsets are all within 3.5 °C, which are consistent with other parts of the QTP but much smaller than in the Arctic and subarctic regions with close-adhered and dense vegetation and the thick, long

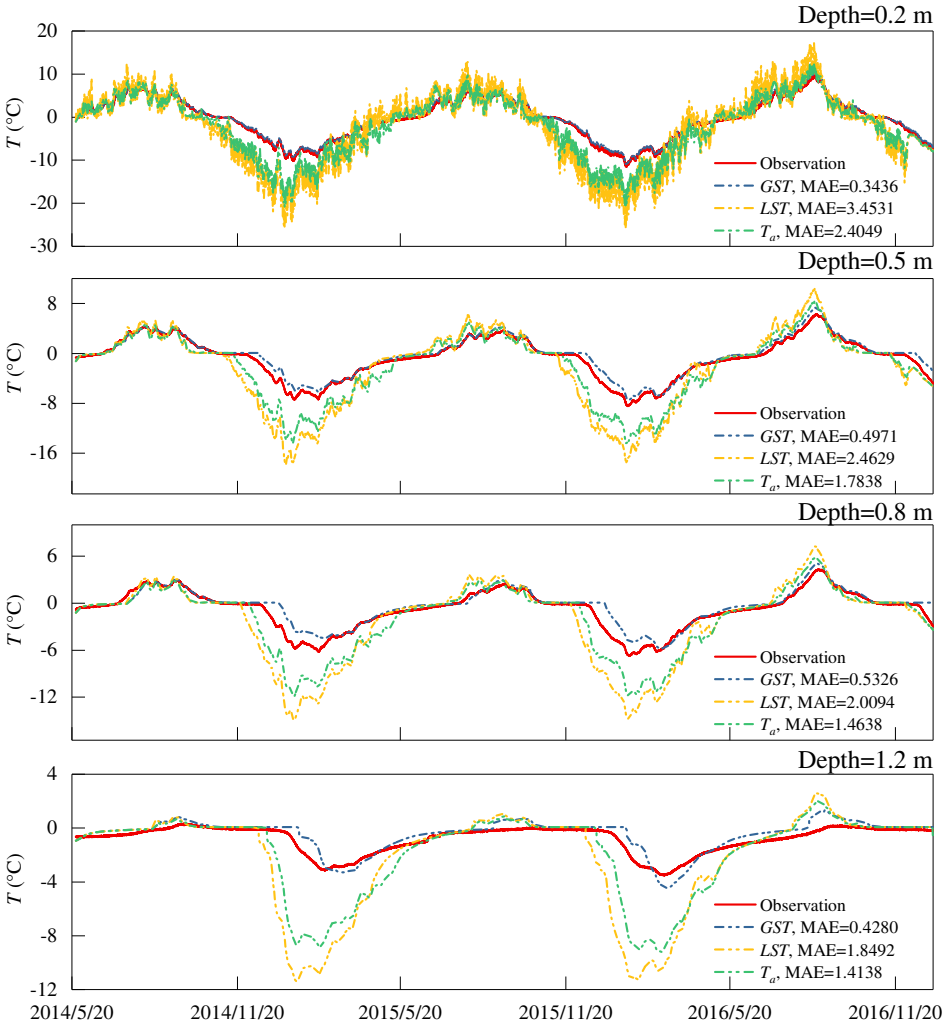

Fig. 8. Measured and simulated ground temperature at depths of 0.2, 0.5, 0.8 and 1.0 m at HRQ2.

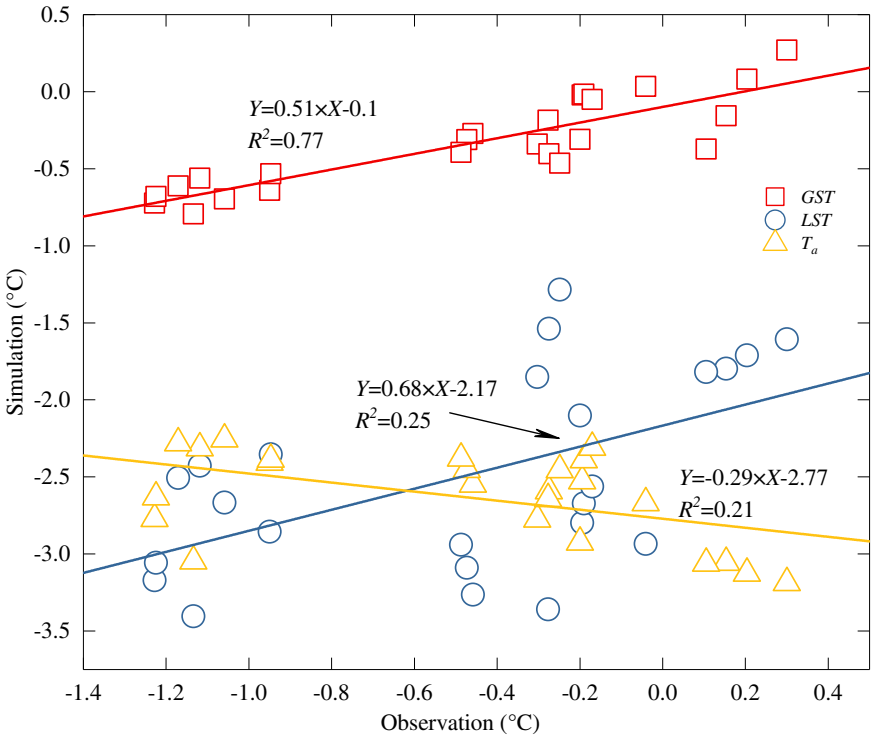

Fig. 9. Simulated and measured MAGTs at depths of 0.2 m, 0.5 m, 0.8 m and 1.0 m during 2015.

duration of snow cover. Thermal offsets are all within 0.3 °C and even reversed, which are relevant to the moderately comparable thawed and frozen thermal conductivities of the soils that consist of fine-grained layers with a small moisture content. Surface characteristics also exert great influence on the freezing and thawing processes of the active layer. Even at the same basin with comparable T_a, freezing and thawing processes are different at HRQ1 and HRQ2.

Simulated results based on the GLPL model demonstrated that the *GST* (0–5 cm subsurface) is a reliable driving parameter to simulate the permafrost temperatures, even without considering the thermal effect of surface characteristics. Simulations based on *LST* or T_a, ignoring the thermal effect of surface characteristics, result in the mean annual values between the simulations and observations being as different as 3 °C. Therefore, the consideration of the thermal effect of surface characteristics is essential to simulate the thermal regime of permafrost based on T_a and the *LST* remote sensing products. In some cases, the *N*-factor, the ratio of *GST* to T_a, could be indirectly replaced to obtain the *GST* to simulate the thermal regime of permafrost, especially for the regions with rugged topography. In the future, ongoing efforts to investigate the thermal effect of surface characteristics on the ground and the quantitatively spatiotemporal relationships among *LST*, T_a and *GST* should improve the modeling or mapping of permafrost on the QTP. Moreover, although there is no stable solid precipitation due to the strong solar radiation on the QTP, frequent accumulation and melting of snow water equivalent with snowfall may exert great influences on the underlying frozen ground. Therefore, accurate *in situ* observations and simulations of snowfall and the melting of snow should also be carried out for better understanding of the influence of surface characteristics on permafrost on the QTP.

Acknowledgments

We thank the Editor and the anonymous reviewers for constructive and detailed comments on the manuscript. We also thank Dr. Ruixia He, Dr. Chengsong Yang and Mr. Shuguang Yang for the soil properties analyses. This research is supported by National Natural Science Foundation of China (NSF) (41671060), the Key Research Program of Chinese Academy of Sciences (CAS) (No. KZZD-EW-13), National Natural Science Foundation of China (NSF) (41401080, 41301068), and the Research Program of State Key Laboratory of Frozen Soil Engineering of Northwest Institute of Eco-Environment and Resources, Chinese Academy of Sciences (SKLFSE-ZT-38).

References

Bense, V.F., Read, T., Verhoef, A., 2016. Using distributed temperature sensing to monitor field scale dynamics of ground surface temperature and related substrate heat flux. Agric. For. Meteorol. 220, 207–215.

Carlson, H.S., 1952. Calculation of depth of thaw in frozen ground. In: Frost Action in Soils: A Symposium Highway Research Board Special Report 2. National Research Council, Washington, DC, pp. 192–223.

Cheng, G.D., 2004. Influences of local factors on permafrost occurrence and their implications for Qinghai-Xizang Railway design. Sci. China Earth Sci. 47 (8), 704–709.

Cheng, W.M., Zhao, S.M., Zhou, C.H., Chen, X., 2012. Simulation of the decadal permafrost distribution on the Qinghai-Tibet Plateau (China) over the past 50 years. Permafr. Periglac. Process. 23, 292–300.

Etzelmüller, B., 2013. Recent advances in mountain permafrost research. Permafr. Periglac. Process. 24, 99–107.

Førland, E.J., Skaugen, T.E., Benestad, R.E., Hanssen-Bauer, I., Tveito, O.E., 2004. Variations in thermal growing, heating, and freezing indices in the Nordic Arctic, 1900–2050. Arct. Antarct. Alp. Res. 36 (3), 347–356.

Fukui, K., Sone, T., Yamagata, K., Otsuki, Y., Sawada, Y., Vetrova, V., Vyatkina, M., 2008. Relationships between permafrost distribution and surface organic layers near Esso, central Kamchatka, Russian Far East. Permafr. Periglac. Process. 19, 85–92.

Goodrich, L.E., 1978. In: Some results of a numerical study of ground thermal regimes, Third International Conference on Permafrost. Proceedings of the 3rd International Conference on Permafrost. National Research Council, Edmonton, Alberta, Canada, pp. 29–34.

Gruber, S., 2012. Derivation and analysis of a high-resolution estimate of global permafrost zonation. Cryosphere 6 (1), 221–233.

Hachem, S., Allard, M., Duguay, C., 2009. Using the MODIS land surface temperature product for mapping permafrost: an application to Northern Quebec and Labrador, Canada. Permafr. Periglac. Process. 20, 407–416.

Hasler, A., Geertsema, M., Foord, V., Gruber, S., Noetzli, J., 2015. The influence of surface characteristics, topography and continentality on mountain permafrost in British Columbia. Cryosphere 9 (3), 1025–1038.

Jafarov, E.E., Romanovsky, V.E., Genet, H., McGuire, A.D., Marchenko, S.S., 2013. The effects of fire on the thermal stability of permafrost in lowland and upland black spruce forests of interior Alaska in a changing climate. Environ. Res. Lett. 8 (3), 035030.

Jin, H.J., He, R.X., Cheng, G.D., Wu, Q.B., Wang, S.L., Lü, L.Z., Chang, X.L., 2009. Changes in frozen ground in the Source Area of the Yellow River on the Qinghai–Tibet Plateau, China, and their eco-environmental impacts. Environ. Res. Lett. 4 (4), 045206.

Karunaratne, K.C., Burn, C.R., 2004. Relations between air and surface temperature in discontinuous permafrost terrain near Mayo, Yukon Territory. Can. J. Earth Sci. 41 (12), 1437–1451.

Klene, A.E., Nelson, F.E., Hinkel, K.M., 2013. Urban–rural contrasts in summer soil-surface temperature and active-layer thickness, Barrow, Alaska, USA. Polar Geogr. 36 (3), 183–201.

Li, J., Sheng, Y., Wu, J.C., Feng, Z.L., Ning, Z.J., Hu, X.L., Zhang, X.M., 2016. Landform-related permafrost characteristics in the source area of the Yellow River, eastern Qinghai-Tibet Plateau. Geomorphology 269, 104–111.

Lin, Z.J., Burn, C.R., Niu, F.J., Luo, J., Liu, M.H., Yin, G.A., 2015. The thermal regime, including a reversed thermal offset, of arid permafrost sites with variations in vegetation cover density, Wudaoliang Basin, Qinghai-Tibet Plateau. Permafr. Periglac. Process. 26, 142–159.

Lunardini, V.J., 1978. In: Theory of n-factors and correlation of data. Proc 3rd Int Conf on Permafrost. NRC, Canada, pp. 40–46.

Luo, D.L., Jin, H.J., Lin, L., You, Y.H., Yang, S.Z., Wang, Y.P., 2013. Distributive features and controlling factors of permafrost and the active layer thickness in the Bayan Har Mountains along the Qinghai-Kangding Highway on northeastern Qinghai-Tibet Plateau. Sci. Geogr. Sin. 33 (5), 635–640 (in Chinese).

Luo, D.L., Jin, H.J., Jin, R., Yang, X.G., Lü, L.Z., 2014. Spatiotemporal variations of climate warming in northern Northeast China as indicated by freezing and thawing indices. Quat. Int. 349, 187–195.

Marchenko, S., Romanovsky, V., Tipenko, G., 2008. In: Numerical modeling of spatial permafrost dynamics in Alaska. Proc 8th Int Conf Permafrost. Wiley, Institute of Northern Engineering, University of Alaska, pp. 190–204.

Muller, S.W., French, H., Nelson, F., 2008. Frozen in Time: Permafrost and Engineering Problems. American Society of Civil Engineers.

Nicolsky, D.J., Romanovsky, V.E., Romanovskii, N.N., Kholodov, A.L., Shakhova, N.E., Semiletov, I.P., 2012. Modeling sub-sea permafrost in the East Siberian Arctic Shelf: the Laptev Sea region. J. Geophys. Res. 117 (F3), F03028.

Pan, X.C., Li, Y.P., Yu, Q.H., Shi, X.G., Yang, D.Q., Roth, K., 2016. Effects of stratified active layers on high-altitude permafrost warming: a case study on the Qinghai–Tibet Plateau. Cryosphere 10 (4), 1591–1603.

Pollack, H.N., Hurter, S.J., Johnson, J.R., 1993. Heat flow from the Earth's interior: analysis of the global data set. Rev. Geophys. 31 (3), 267–280.

Ran, Y.H., Li, X., Jin, R., Guo, J.W., 2015. Remote sensing of the mean annual surface temperature and surface frost number for mapping permafrost in China. Arct. Antarct. Alp. Res. 47 (2), 255–265.

Riseborough, D., Shiklomanov, N., Etzelmuller, B., Gruber, S., Marchenko, S., 2008. Recent advances in permafrost modelling. Permafr. Periglac. Process. 19 (2), 137–156.

Romanovsky, V.E., Osterkamp, T.E., 1995. Interannual variations of the thermal regime of the active layer and near-surface permafrost in northern Alaska. Permafr. Periglac. Process. 6, 313–335.

Smith, M.W., 1975. Microclimatic influences on ground temperatures and permafrost distribution, Mackenzie Delta, Northwest Territories. Can. J. Earth Sci. 12 (8), 1421–1438.

Smith, M.W., Riseborough, D.W., 2002. Climate and the limits of permafrost: a zonal analysis. Permafr. Periglac. Process. 13, 1–15.

Smith, S.L., Burgess, M.M., Riseborough, D., Mark Nixon, F., 2005. Recent trends from Canadian permafrost thermal monitoring network sites. Permafr. Periglac. Process. 16, 19–30.

Tedesco, M., 2015. Remote Sensing of the Cryosphere. John Wiley & Sons.

Wang, B.L., French, H.M., 1994. Climate controls and high-altitude permafrost, Qinghai-Xizang (Tibet) Plateau, China. Permafr. Periglac. Process. 5, 87–100.

Willmott, C.J., Matsuura, K., 2005. Advantages of the mean absolute error (MAE) over the root mean square error (RMSE) in assessing average model performance. Clim. Res. 30 (1), 79–82.

Wu, T.H., Zhao, L., Li, R., Wang, Q.X., Xie, C.W., Pang, Q.Q., 2013. Recent ground surface warming and its effects on permafrost on the central Qinghai-Tibet Plateau. Int. J. Climatol. 33 (4), 920–930.

Xu, X.Z., Wang, J.C., Zhang, L.X., 2010. Physics of Frozen Soils (in Chinese). Science Press, Beijing.

Yershov, E.D., 2004. In: Williams, P.J. (Ed.), General Geocryology. Cambridge university press, The Pitt Building, Trumpington Street, Cambridge, United Kingdom.

Yin, G.A., Niu, F.J., Lin, Z.J., Luo, J., Liu, M.H., 2017. Effects of local factors and climate on permafrost conditions and distribution in Beiluhe basin, Qinghai-Tibet Plateau, China. Sci. Total Environ. 581-582, 472–485.

Zhang, T.J., Barry, R.G., Knowles, K., Heginbottom, J.A., Brown, J., 2008. Statistics and characteristics of permafrost and ground-ice distribution in the Northern Hemisphere. Polar Geogr. 31 (1–2), 47–68.

Zhou, Y.W., Qiu, G.Q., Guo, D.X., Cheng, G.D., Li, S.X., 2000. Geocryology in China (in Chinese). Science Press, Beijing.